ARTICLES
PUBLISHED ONLINE: 28 APRIL 2013 | DOI: 10.1038/NPHYS2610
nature physics

Long-range magnetic order in a purely organic 2D layer adsorbed on epitaxial graphene

Manuela Garnica[1,2†], Daniele Stradi[2,3†], Sara Barja[1,2], Fabian Calleja[2], Cristina Díaz[3], Manuel Alcamí[3], Nazario Martín[2,4], Amadeo L. Vázquez de Parga[1,2*], Fernando Martín[2,3] and Rodolfo Miranda[1,2]

Collective magnetic properties are usually associated with the *d* or *f* electrons that carry the individual magnetic moments. A fully spin-polarized ground state based on π electrons has been predicted in half-filled flat-band organic materials, but has remained experimentally challenging to realize. Here we show that isolated tetracyano-*p*-quinodimethane molecules deposited on graphene epitaxially grown on Ru(0001) acquire charge from the substrate and develop a magnetic moment of 0.4 μ_B per molecule. The magnetic moment survives even when the molecules form into a dimer or a monolayer, with a value of 0.18 μ_B per molecule for the monolayer. The self-assembled molecular monolayer develops spatially extended spin-split electronic bands, and we visualized the ground-state spin alignment using spin-polarized scanning tunnelling microscopy. The observation of long-range magnetic order in an organic layer adsorbed on graphene paves the way for incorporating magnetic functionalities into graphene.

Much effort is being devoted to combining the properties of organic magnets and graphene because adding magnetic functionalities to graphene will not only complement its extraordinary electronic, mechanic and optical properties, but also open the way to graphene-based spintronics. Organic metals and magnets rely on charge-transfer processes to create either the metallic character or the magnetic properties. Thus, the prototype all-organic conductor consists of alternate columnar stacks of TCNQ (7,7′,8,8′-tetracyano-*p*-quinonedimethane) and TTF (tetrathiafulvane). It is a one-dimensional (1D) charge-transfer complex[1] in which each TTF molecule donates 0.6 electrons to TCNQ. The compound has a high conductivity at 300 K ($\sim$400 S cm^{-1}; ref. 2), but becomes insulating below 60 K owing to a Peierls transition in its quasi-1D structure[3]. Similarly, the first organic-based magnets with Curie temperatures $T_c = 4.8$ K (ref. 4) or $T_c = 13$ K (for example, Ni(TCNQ)$_2$; ref. 5) and the metal organic magnets with the highest T_c (above 350 K; ref. 6) are electron transfer salts consisting of strong organic acceptors, such as tetracyanoethylene (TCNE) or TCNQ, that receive charge from metallic donors (for example, V or Ni). The long-range magnetic order in (TCNE)V_2 is due to the antiferromagnetic coupling between the localized spins on the metal ions and the radical organic anions[6].

Here we show that TCNQ molecules deposited on graphene grown on Ru(0001) acquire charge and develop a sizeable magnetic moment that is preserved on monolayer formation. The self-assembled 2D monolayer of TCNQ molecules adsorbed on graphene develops long-range magnetic order in the ground state with spatially extended spin-split electronic bands. This is possible because graphene, which does not react with the deposited TCNQ molecules, prevents the formation of TCNQ–Ru(0001) bonds while allowing efficient charge transfer from the graphene/Ru(0001) substrate to the molecules. This large charge transfer, in turn, is the consequence of the strong interaction of graphene with the Ru(0001) substrate and its subsequent doping from this substrate, but it should also be attainable for a gated graphene layer deposited on an insulator.

Ultraperfect graphene[7] monolayers can be epitaxially grown on many single-crystal metal surfaces under ultrahigh vacuum (UHV) conditions[8,9]. Often these graphene layers are spontaneously nanostructured, forming a periodic array of nanoripples caused by the difference in the lattice parameter between graphene and the different substrates[8,9]. The lateral periodicity of the ripples is 2–3 nm depending on the metal substrate. Graphene epitaxially grown on Ru(0001)[9], in particular, is a system that has attracted widespread attention. The graphene monolayer in this case is doped with electrons from the metal underneath. *In situ* scanning tunnelling microscope (STM) imaging of the graphene monolayers reveals that, in addition to the structural corrugation, a much stronger electronic corrugation exists[9,10], rendering this rippled graphene layer a nanostructured playground for ordered molecular adsorption[11,12].

The TCNQ molecules were deposited on graphene/Ru(0001) at 300 K and imaged with STM at 4.6 K. Figure 1a shows individual TCNQ molecules that always adsorb at the lower part of the ripples, where the total charge density is larger and the surface potential is lower. Contrary to what happens when TCNQ is deposited on most metallic surfaces[13], the topographic STM images show intramolecular resolution that changes with the bias voltage applied between the tip and the sample.

The adsorption geometry and the electronic structure of isolated TCNQ molecules deposited on rippled graphene on Ru(0001) has been calculated from first principles by using density functional theory (DFT) as implemented in the VASP (Vienna *ab initio* simulation package) code[14,15] (see Supplementary Information A1 for details of the calculations). The simulated

[1]Departamento Física de la Materia Condensada, Universidad Autónoma de Madrid, Cantoblanco 28049, Madrid, Spain, [2]Instituto Madrileño de Estudios Avanzados en Nanociencia (IMDEA-Nanociencia), Cantoblanco 28049, Madrid, Spain, [3]Departamento de Química Módulo 13, Universidad Autónoma de Madrid, Cantoblanco 28049, Madrid, Spain, [4]Facultad de Química, Universidad Complutense de Madrid, 28040, Madrid, Spain. †These authors contributed equally to this work. *e-mail: al.vazquezdeparga@uam.es

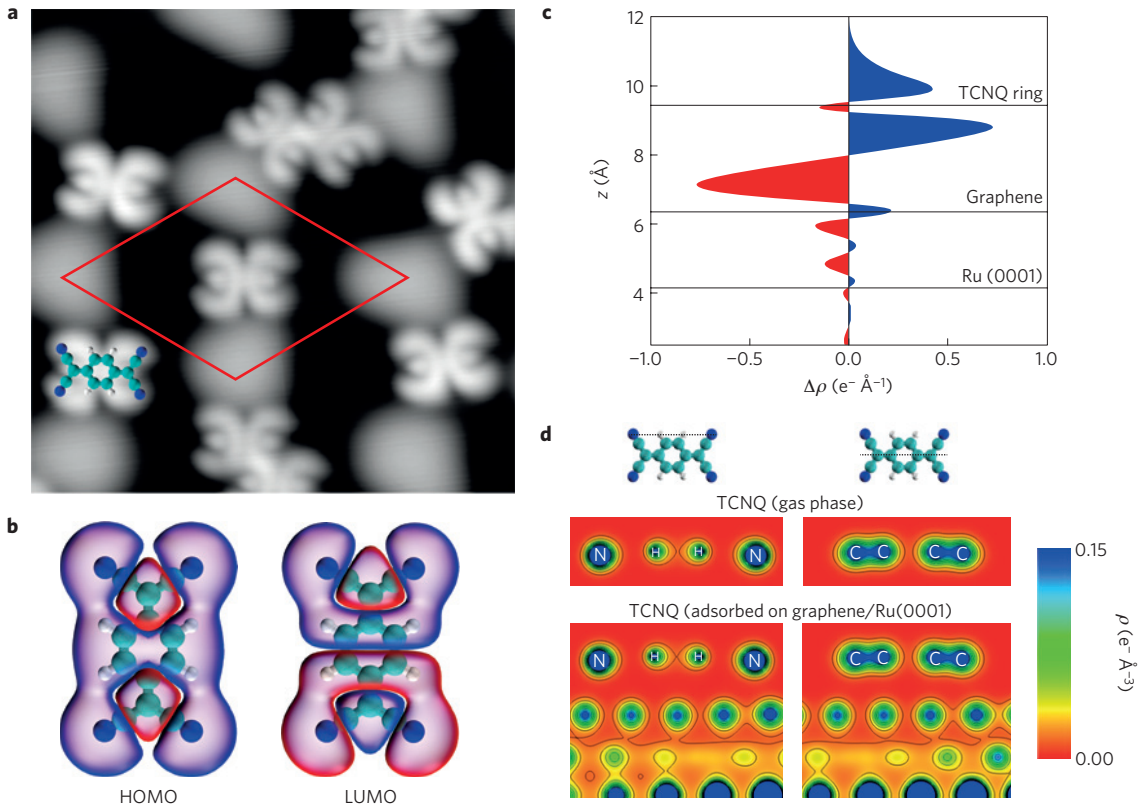

Figure 1 | Adsorption geometry and charge transfer for individual TCNQ molecules on graphene on Ru(0001). a, $8 \times 8\,nm^2$ STM image of individual TCNQ molecules adsorbed on graphene/Ru(0001) ($V_b = -0.8$ V, $I_t = 50$ pA) measured at 4.6 K. The white blobs are the upper part of the moiré pattern of graphene/Ru(0001) whose unit cell is also indicated. **b**, Calculated HOMO and LUMO of TCNQ in the gas phase superimposed on the atomic structure. Carbon, nitrogen and hydrogen atoms of TCNQ are coloured in cyan, blue and white, respectively. **c**, Calculated electronic density redistribution $\Delta\rho$ (averaged in the x-y-plane) on adsorption of isolated TCNQ on graphene/Ru(0001). Blue indicates electronic density accumulation; red indicates electronic density depletion. **d**, The lower panels show 2D cuts of the electronic charge density $\rho(r)$ in the direction perpendicular to the x-y-plane for the adsorption configuration of TCNQ. The two cuts are indicated by dotted lines in the upper part of the panel. The central part shows the charge distribution for a free-standing, charged TCNQ molecule. Note that the charge distribution is identical for the adsorbed and the free-standing, but charged molecule.

graphene/Ru(0001) substrate accounts for the observed moiré pattern and provides an accurate representation of the apparent corrugation of graphene/Ru(0001) at different bias voltages[16] as well as of scanning tunnelling spectroscopy spectra near and well above the Fermi level[9,10,17]. Theoretical results show a substantial charge transfer from Ru to graphene.

The lower part of the moiré ripples constitutes a preferential adsorption site for strong acceptors, such as TCNQ molecules, which are found to adsorb with a large adsorption energy (2.37–2.53 eV per molecule), depending on the particular adsorption site and configuration. The energy difference between different configurations in each low area of the moiré is less than 50 meV, in agreement with the experimental observation that there is no preferential adsorption configuration for isolated molecules within the lower areas of the moiré (see Supplementary Fig. S1). The TCNQ–graphene distance is about 3 Å. Figure 1b shows the shape of the calculated highest occupied molecular orbital (HOMO) and lowest unoccupied molecular orbital (LUMO) of TCNQ in the gas phase. Note the presence of a node in the wavefunction of the LUMO orbital and its similarity to the molecular shape observed experimentally. As the STM image of Fig. 1a corresponds to occupied states, it indicates that the previously empty LUMO orbital is now partly occupied.

The calculations for individual TCNQ molecules adsorbed on graphene/Ru(0001) reveal indeed that there is a substantial charge transfer from graphene to TCNQ, whereas the Ru substrate is essentially unaffected. Figure 1c shows the electronic density redistribution integrated over the X–Y plane. About one complete electron is transferred from the graphene sheet to the molecule. This is confirmed by an estimation based on Bader's analysis of the charge density[18]: the predicted charge per molecule is 0.99 electrons. Figure 1d shows two vertical cuts of the charge density for TCNQ adsorbed on graphene/Ru(0001) (lower panels) compared to the charge density for a gas-phase, singly charged TCNQ molecule (upper panels). It can be seen that the electronic charge distribution at the TCNQ molecule is identical in both cases and there is no sizeable charge density accumulation in the region between the molecule and the surface. Both facts indicate that the effect of the interaction with the graphene/Ru(0001) substrate is essentially the charging of the molecule. Note that this is so in spite of the fact that ruthenium 4d orbitals are explicitly included in the calculations[16]. Decoupling of the electronic states of an adsorbed molecule from the substrate was previously observed for NaCl ultrathin layers[19].

Thus, graphene, which is n-doped from the interaction with the Ru substrate, efficiently transfers electrons to TCNQ. A more detailed analysis shows that the additional charge density mainly goes into the LUMO of the neutral molecule, which splits into a single occupied molecular orbital (SOMO) and a single unoccupied molecular orbital (SUMO). dI/dV spectroscopy at the single-molecule level allows us to identify the maximum of the HOMO at −2.0 V (sample bias) and provides an unequivocal confirmation of the existence of an occupied SOMO orbital around −0.8 V. The experimental identification of the molecular states is employed to record spatially resolved dI/dV maps. The spectroscopic STM

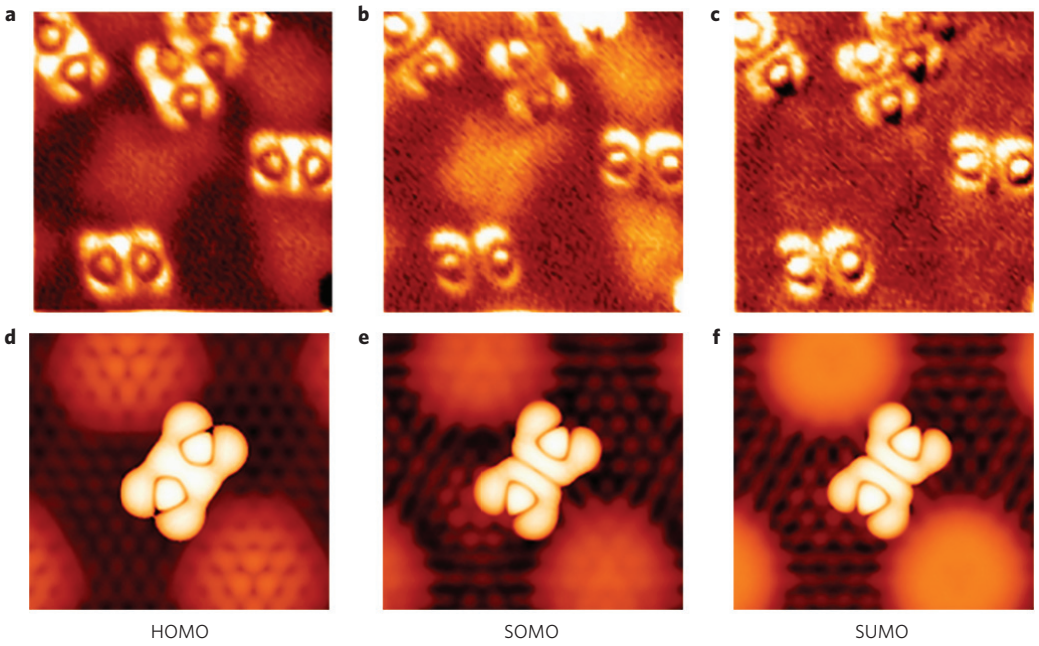

Figure 2 | Spatial distribution of the molecular frontier orbitals for TCNQ adsorbed on graphene/Ru(0001). a–c, Spatially resolved dI/dV maps of individual TCNQ molecules adsorbed on graphene/Ru(0001) recorded at $V_b = -2$ V (**a**), $V_b = -0.8$ V (**b**) and $V_b = +1.0$ V (**c**). **d–f**, The corresponding simulated dI/dV maps.

maps of the HOMO (recorded at −2.0 V), SOMO (at −0.8 V) and SUMO (at +1.0 V) orbitals of isolated TCNQ molecules deposited on graphene/Ru(0001) are shown in the upper row in Fig. 2. Note that whereas the HOMO does not show a node in the central plane of the molecule, both the SOMO and the SUMO clearly exhibit the characteristic central node. The shape of these two, in fact, is practically identical, indicating that they originate from the same, previously empty LUMO orbital. The lower row of Fig. 2 shows the calculated images of the local density of states of the adsorbed TCNQ molecule in the corresponding range of energy. The agreement between the simulated and the measured spectroscopy maps is striking for all HOMO, SOMO and SUMO levels, confirming the accuracy of the simulation in predicting the localization of the unpaired electron transferred from graphene to the π molecular orbital derived from the LUMO.

Figure 3a,b shows the spin-density distribution and the projected density of states (PDOS) resulting from a spin-polarized calculation for a single TCNQ molecule on its optimized adsorption geometry on graphene/Ru(0001). The (now partially occupied) LUMO orbital splits into spin-up SOMO and spin-down SUMO with different filling ratios. The energy width of the orbitals is determined by the interaction with the substrate. In agreement with the different electron occupancy (the spin-up SOMO is more than half-filled and the spin-down orbital less than half-filled) the adsorbed TCNQ molecule develops a magnetic moment of approximately 0.4 μ_B. The spin density is distributed across the entire orbital as indicated by Fig. 3a. Note that our spin-polarized gas-phase calculations show, as expected, that TCNQ has HOMO and LUMO states without magnetic splitting.

To test experimentally the prediction of the appearance of a magnetic moment in isolated TCNQ molecules, we resort to the observation of the Kondo effect by scanning tunnelling spectroscopy. The Kondo effect[20] reflects the screening of the spin of magnetic impurities by the conduction electrons of non-magnetic metals that results in a many-body ground state below the Kondo temperature, T_K. The Kondo resonance appears as a sharp feature at the Fermi level in differential conductance (dI/dV) spectra recorded on top of magnetic impurities[21–29]. Although this feature is a dip for magnetic impurities strongly coupled to the substrate[21–24], there is a growing body of evidence that it might also appear as a sharp peak if the magnetic impurity is weakly coupled to the substrate, as often occurs for adsorbed molecules with a magnetic moment[25–29].

Figure 3d shows dI/dV spectra measured with the STM tip held on top of the TCNQ molecule (red) and on graphene (black) as indicated in Fig. 3c. A sharp peak at zero bias is observed when the STM tip is located on top of the cyano groups of the TCNQ molecules. dI/dV spectra measured in the neighbouring graphene surface (black curve) do not show any special feature at the Fermi level. The narrow width of this peak rules out a molecular resonance as the origin of this peak (see for comparison the width of the molecular orbitals shown in Supplementary Fig. S9). Its intensity exhibits a strong dependence on the STM tip position in the TCNQ molecule (see Supplementary Information SI-C for details). The line-shape dependence on the temperature of this peak behaves as expected for a Kondo resonance[23] and it is comparable to the one measured by means of STM in other magnetic molecules deposited on metallic substrates[25,27,28]. We identify it as a Kondo resonance due to the interplay between the conduction electrons of graphene/Ru(0001) and the magnetic moment associated with the TCNQ molecules. According to our calculations, the Kondo scenario develops because the transfer of a second electron from the graphene/Ru(0001) substrate to the magnetic TCNQ radical anion is forbidden by its corresponding electron affinity being well above the Fermi level of graphene/Ru(0001). The peak can be fitted with a Fano line shape (shown in blue in Fig. 3d) with a full-width at half-maximum of 10 ± 1 mV giving a Kondo temperature of 60 K. The observation of the Kondo resonance confirms that isolated TCNQ molecules have acquired a magnetic moment because of the electrons transferred from graphene/Ru(0001). Although the existence of unpaired electrons in organic molecules is a prerequisite to molecular magnetism, their mutual interactions are required to develop long-range magnetic order in molecular materials.

A larger coverage of TCNQ produces the formation of dimers and trimers (see Supplementary Information SI-D) and, later,

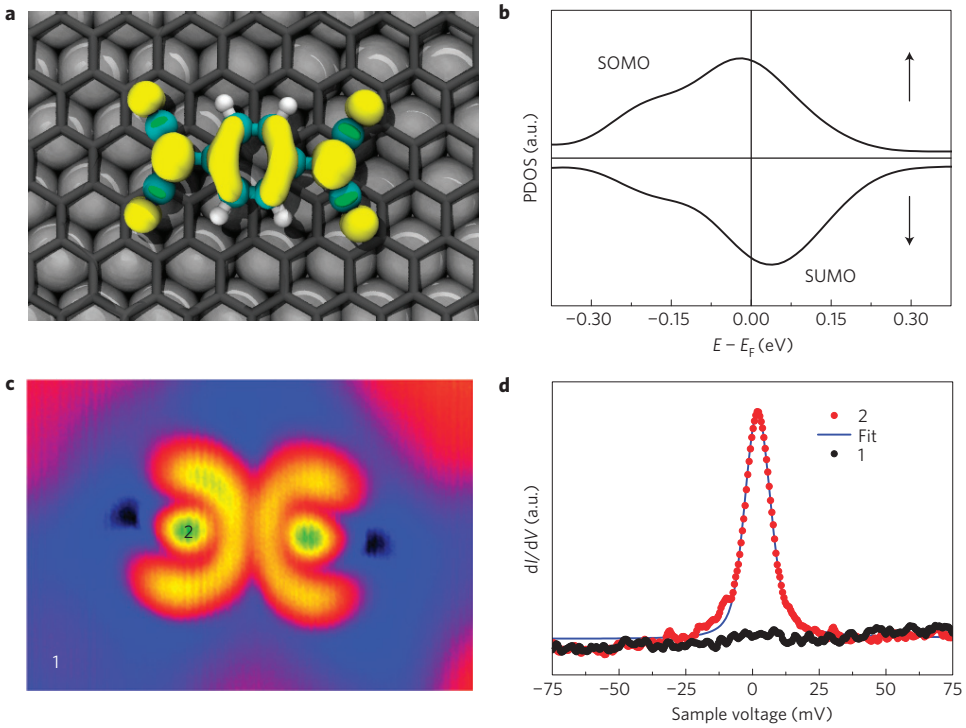

Figure 3 | Magnetic moment and Kondo resonance for individual TCNQ molecules. a, Calculated spin-density distribution for a single TCNQ molecule adsorbed on graphene/Ru(0001). Yellow and green indicate positive and negative spin densities, respectively. **b**, Calculated spin-polarized PDOS over *s* and *p* orbitals for the same molecule. **c**, Topographic STM image (3 nm × 1.5 nm, $V_b = -0.3$ V, $I_t = 70$ pA) of a TCNQ molecule on graphene/Ru(0001) with the numbers indicating the spatial location where the spectra in **d** have been recorded. **d**, Differential conductance, dI/dV, spectra measured with the STM tip held on the TCNQ molecule and on graphene. The blue line shows the fit to a Fano line shape $(q+\varepsilon)^2/1+\varepsilon^2$, with $q = 40$ and $\varepsilon = 1.7$. All the measurements were carried out with the sample at 4.6 K.

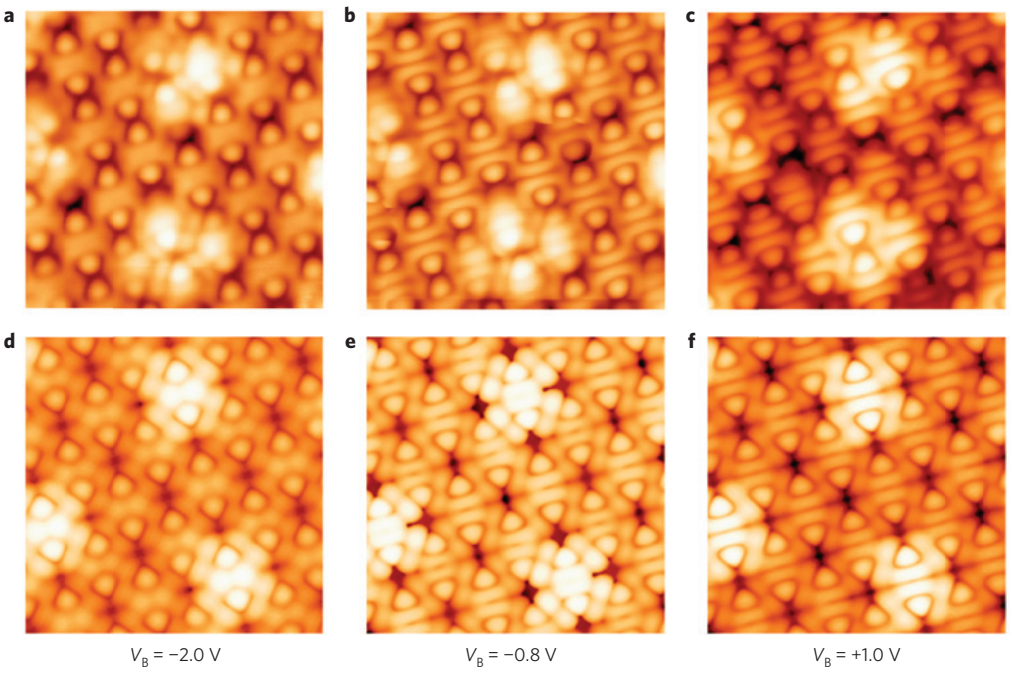

Figure 4 | Spatially extended intermolecular bands in a TCNQ monolayer adsorbed on graphene/Ru(0001). a–**c**, Topographic STM images of a TCNQ monolayer on graphene/Ru(0001) recorded at $V_b = -2$ V (**a**), $V_b = -0.8$ V (**b**) and $V_b = +1.0$ V (**c**). **d**–**f**, The corresponding simulated topographic images. The bands result from the hybridization of the TCNQ frontier orbitals.

the decoration of all the lower areas of the ripples, before the formation of a full monolayer with molecules also forced to occupy the upper part of the ripples. Both calculations and experiments (see Supplementary Information SI-E) indicate that the magnetic moment developed in the TCNQ monomer is preserved on the formation of dimers, trimers and so on.

The TCNQ monolayer adsorbed on graphene/Ru(0001) has been simulated by using a (11×11) graphene/(10×10) Ru(0001) supercell[16] containing eight TCNQ molecules. After optimization of the geometry of the monolayer, the adsorption energy is found to be 1.88 eV per molecule and the charge transfer is of the order of 0.4–0.6 electrons per molecule. The average TCNQ–graphene distance is the same as in the case of a single TCNQ molecule adsorbed on graphene/Ru(0001). STM imaging of the full monolayer reveals striking differences as a function of the bias voltage: the images recorded at the HOMO energy (−2.0 V; Fig. 4a) differ substantially from those corresponding to the SOMO (−0.8 V; Fig. 4b) and SUMO (+1.0 V; Fig. 4c) energies. The last two are again almost identical to each other. As illustrated in Fig. 4b,c, the experimental images show well-resolved, tube-like structures separated by clear nodes, corresponding to TCNQ intermolecular states that extend over the whole surface. The tubes reflect the real-space imaging of the occupied (and empty) intermolecular bands below (and above) the Fermi level. The simulated constant-current STM images reproduce almost exactly the experimental ones for the HOMO, SOMO and SUMO orbitals, including the higher resolution of the orbital nodes observed for TCNQ molecules on the lower part of the ripples compared with the ones at the higher parts, as can be seen in Fig. 4d–f.

The spin-polarized calculations for the TCNQ monolayer adsorbed on graphene/Ru(0001) show that the magnetically ordered structure is energetically favoured. The total calculated magnetic moment per unit cell (containing 8 molecules) is 1.3 μ_B; that is, an average magnetic moment per molecule of 0.18 μ_B. An analysis of the spin density indicates that this magnetic moment is due to unpaired electrons in the SOMO-derived band. To understand the physics behind these findings, avoiding the complexity (and size) of the real system we have used a simpler but realistic model consisting of a free-standing TCNQ monolayer with the same corrugated geometry as the adsorbed one and different degrees of added charge to simulate the charge transferred from the graphene/Ru(0001) substrate. Table 1 summarizes the results for a monolayer charged with 0.5 electrons per molecule: the layer is magnetically ordered with a magnetic moment of 0.23 μ_B per molecule and an energy gain of around 50 meV per unit cell. Our calculations also show that the conclusion is robust; that is, the magnetically ordered solution for the TCNQ monolayer is always the most stable one, in the range of charge filling relevant to our experimental system (0.3–0.6 electrons per molecule; see Supplementary Information SI-F).

According to our calculations, the intermolecular bands observed in Fig. 4 in real space are also very similar to those of a planar, free-standing, charged TCNQ monolayer (see Supplementary Fig. S6B). For the latter, the corresponding bands in the reciprocal space are almost flat and have a magnetic character revealed by the analysis of their electronic structure: the spin-up component of the SOMO-derived band is almost completely filled, whereas the spin-down counterpart (SUMO-derived) is rather empty. A system with a half-filled (nearly) flat band is predicted to have a ferromagnetic ground state. This was rigorously demonstrated in refs 30,31 for various classes of Hubbard models following the initial demonstration in ref. 32. The possibility of band ferromagnetism in a purely organic polymer that survives the Peierls instability was recently demonstrated theoretically[33]. Organics exhibiting single-band long-range magnetic order, however, have yet to be synthesized. Our spin-polarized calculation suggests that TCNQ/graphene/Ru(0001) might be such a system.

We have employed spin-polarized STM (ref. 34) at low temperature to test these predictions in samples containing different molecular domains. To this end, the W tip of the STM has been coated *in situ* with a thin film of Fe, which provides in-plane, spin-sensitive contrast. The different orientation of adsorbed TCNQ with respect to the graphene lattice allows the existence of magnetic domains with the axis of the molecules defined by the intermolecular bands. The spin-polarized contribution to the tunnelling current is associated to a non-zero in-plane component of the sample magnetization, which should change direction when going from one domain to the other. As the spin-polarized contribution to the tunnelling current depends on the angle between the sample and tip magnetizations[34], one should thus expect different current intensities in different domains for a given tip magnetization direction. In our system the SUMO- and SOMO-derived bands are spin split and, therefore, the spin-polarized differential tunnelling conductance will be enhanced (reduced) at the bias voltage that corresponds to the energy of the molecular band with spin parallel (antiparallel) to the tip's preferred spin direction.

Table 1 | Magnetic moments per molecule and relative energies per unit cell, ΔE, of different magnetic configurations for a free-standing TCNQ monolayer charged with 0.5 electrons per molecule.

Configuration	M (μ_B) per molecule	$\Delta E = E_{Configuration} - E_{NM}$ (meV)
NM	0.0 (0.0)	0.0 (0.0)
HS	0.5 (0.5)	−105.1 (−106.6)
Free	0.24 (0.24)	−53.90 (−52.40)

NM, non-magnetic configuration; HS, high-spin configuration; Free, configuration in which the magnetic moments have been allowed to relax without constraints. Data in parentheses refer to the calculations performed using the non-collinear DFT framework, including spin–orbit coupling. See Supplementary Information SI-F for details.

Figure 5a shows a constant-current topographic image of two such domains of TCNQ molecules. In each domain the brighter regions correspond to molecules sitting on the hills of the rippled graphene layer. Figure 5c compares the spin-resolved differential tunnelling conductance averaged over three moiré unit cells (containing more than 30 molecules) measured on the two TCNQ domains simultaneously with the topography. The spin-polarized spectrum shows three characteristic peaks identified as the HOMO- (−1.8 eV), SOMO- (−0.75 eV) and SUMO- (+0.75 eV) derived bands, respectively. The intensity of the spin-resolved differential tunnelling conductance for the spin-polarized SOMO level at −0.7 eV is indeed, as explained above, different in the two domains and opposite in sign to the one measured at the spin-polarized SUMO level (+0.75). This inversion in the contrast between the SUMO and SOMO when going from one domain to the other and the almost identical resolution in the topographic images of both domains exclude the influence in the results of a specific tip termination or a different coupling of the tip states to the molecular orbitals (see also Supplementary Information SI-G). Inside each domain there are periodic differences between the spin-polarized intensity of the SOMO and SUMO orbitals for molecules located on top of the hills and in the valleys (see Supplementary Fig. S10 for a spatially resolved map of the magnetic contrast), but the average intensity of the SOMO (SUMO) orbital in one domain is systematically larger (smaller) than in the other.

Similar results are obtained with dozens of different Fe-coated tips, although the intensity of the spin-polarized signal (of the order of $14 \pm 2\%$ in Fig. 5c) changes slightly from tip to tip owing to the arbitrary orientation of the magnetization of the tip apex with respect to the one of the molecular domains (see Supplementary Fig. S8). A possible influence of the tip stray field in the spin-polarized dI/dV maps cannot be excluded a priori. The stray field, however, will force the magnetization

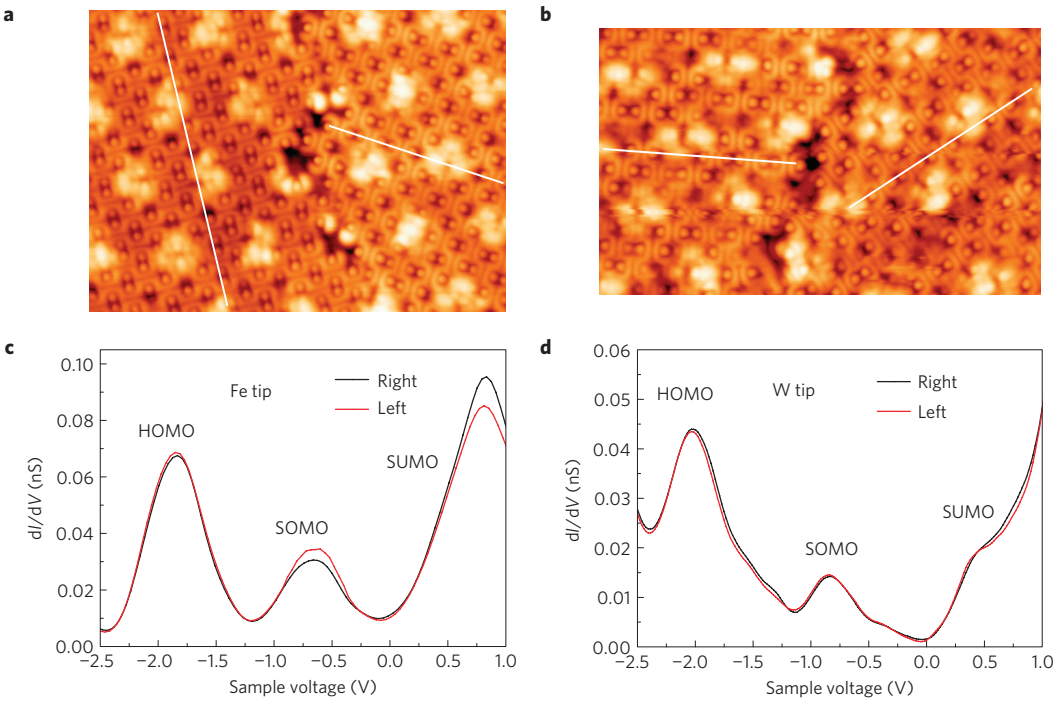

Figure 5 | Spin polarized measurements. a,**b**, STM topographic images (left: 16.7 nm × 12.1 nm^2 and right: 14 × 8.5 nm^2) of a TCNQ monolayer on graphene/Ru(0001) recorded at $V_s = +1.5$ V and $I_t = 100$ pA, left, and $I_t = 50$ pA, right, showing two molecular domains aligned in different directions with respect to the scanning axis. **c**, Spin-polarized dI/dV curves averaged over three unit cells of the moiré superstructure for the left and right domains of **a** (red and black curves respectively). The individual curves have been taken at 4.6 K using an Fe-coated W tip with the tunnelling gap stabilized at $V_s = +1.5$ V and 100 pA. The three peaks correspond to the HOMO (at −1.8 V), SOMO (at −0.7 V) and SUMO (at +0.7 V) bands. **d**, Spin-integrated dI/dV curves averaged over three unit cells of the moiré superstructure for the left and right domains of **b** (red and black curves respectively). The individual curves have been taken at 4.6 K using a W tip with the tunnelling gap stabilized at $V_s = +1.5$ V and 50 pA. The peaks correspond to the HOMO, SOMO and SUMO bands. The white lines in **a**,**b** indicate the long axis of the TCNQ molecules in the molecular domains.

of different domains to align with the tip magnetization, thus reducing the contrast in the spin-polarized dI/dV maps[34]. In our case, if the TCNQ adlayer is paramagnetic, the stray field would align the magnetic moments along its externally imposed direction in both domains, eliminating the contrast. Our results, thus, reveal the existence of magnetic contrast due to long-range magnetic order between the two TCNQ domains. This conclusion is further supported by the observed absence of contrast for the spin-unpolarized HOMO peak at −1.8 eV.

Figure 5b shows a constant-current topographic image of two TCNQ domains measured with a clean W tip. No difference in the intensity of the HOMO, SOMO or SUMO peaks is detected for the differential tunnelling conductance curves recorded in different domains (Fig. 5d).

These observations indicate the existence of long-range magnetic order in the TCNQ adlayer at 4.6 K. A rough estimate of the ordering temperature in the range of 7–10 K can be obtained from the calculated energy difference between the free (magnetically ordered) system and the (forced) non-magnetic state. Our calculations further indicate that the coupling mechanism leading to this long-range magnetic ordering is the intermolecular hybridization of the TCNQ frontier orbitals, which favours direct exchange between the electrons transferred from the substrate to the degenerate, extended, intermolecular bands created by the hybridization (see also Supplementary Information SI-E and SI-F).

On adsorption of TCNQ on rippled graphene/ Ru(0001), each isolated molecule acquires charge from graphene, developing a localized magnetic moment and showing a prominent Kondo resonance. On completion of the TCNQ monolayer, the delocalization on a spatially extended band preserves a common orientation of the electron spins, as revealed by spin-polarized STM. Thus, a magnetically ordered, 2D organic layer has been created by charge donation from graphene/Ru(0001) to the strong acceptor TCNQ (very much akin to charge-transfer complexes). As the added charge occupies spatially extended intermolecular bands with well-defined spin character, one might speculate that the TCNQ monolayer could act as a spin filter or 2D spin polarizer, adding magnetic functionalities to graphene by altering the spin polarization of a current flowing in graphene.

Methods

The graphene/Ru(0001) surface was modelled employing periodic boundary conditions, using the geometry described in ref. 16. The periodic boundary condition calculations have been performed employing DFT, as implemented in the VASP code[14]. Unless otherwise stated, DFT has been used (structures, total energies, charge transfer and STM simulations), and spin-polarized DFT has been used only for the electronic structure analysis (PDOS and spin density).

All experiments were performed in an UHV chamber with a base pressure of 5×10^{-11} mbar equipped with a low-temperature STM and facilities for tip and sample preparation. The graphene layer was prepared by keeping the Ru crystal at 1150 K in UHV while exposing it to an ethylene partial pressure of 8×10^{-8} mbar for 10 min. TCNQ molecules were evaporated from a quartz crucible heated at 350 K with the sample held at room temperature with a deposition rate of 1 layer every four minutes. The clean W tips were prepared by Ar^+ sputtering (2.5 keV) in an UHV for 45 min. For magnetic imaging the tips were covered with iron.

Received 3 October 2012; accepted 15 March 2013; published online 28 April 2013

References

1. Coleman, L. B. *et al.* Superconducting fluctuations and the Peierls instability in an organic solid. *Solid State Commun.* **12,** 1125–1132 (1973).

2. Thomas, G. A. *et al.* Electrical conductivity of tetrathiafulvalenium-tetracyanoquinodimethanide (TTF-TCNQ). *Phys. Rev. B* **13,** 5105–5110 (1976).
3. Peierls, R. *Surprises in Theoretical Physics* (Princeton Univ. Press, 1979).
4. Miller, J. S., Epstein, A. J. & Reif, W. M. Molecular/organic ferromagnets. *Science* **240,** 40–47 (1988).
5. Jain, R. *et al.* High-temperature metal-organic magnets. *Nature* **445,** 291–294 (2007).
6. Manriquez, J. M. *et al.* A room-temperature molecular/organic-based magnet. *Science* **252,** 1415–1417 (1991).
7. Novoselov, K. & Geim, A. Electric field effect in atomically thin carbon films. *Science* **306,** 666–669 (2004).
8. Batzill, M. The surface science of graphene: Metal interfaces, CVD synthesis, nanoribbons, chemical modifications, and defects. *Surf. Sci. Rep.* **67,** 83–115 (2012).
9. Vázquez de Parga, A. L. *et al.* Periodically rippled graphene: Growth and spatially resolved electronic structure. *Phys. Rev. Lett.* **100,** 056807 (2008).
10. Borca, B. *et al.* Potential energy landscape for hot electrons in periodically nanostructured graphene. *Phys. Rev. Lett.* **105,** 036804 (2010).
11. Barja, S. *et al.* Self-organization of electron acceptor molecules on graphene. *Chem. Commun.* **46,** 8198–8200 (2011).
12. Mao, J. *et al.* Tunability of supramolecular Kagome lattices of magnetic Pthalocyanines using graphene-based moiré patterns as templates. *J. Am. Chem. Soc.* **131,** 14136–14137 (2009).
13. Tseng, T. C. *et al.* Charge-transfer-induced structural rearrangements at both sides of organic/metal interfaces. *Nature Chem.* **2,** 374–379 (2010).
14. Kresse, G. & Hafner, J. *Ab-initio* molecular dynamics for liquid metals. *Phys. Rev. B* **47,** 558–561 (1993).
15. Kresse, G. & Joubert, D. From ultrasoft pseudopotentials to the projector augmented-wave method. *Phys. Rev. B* **59,** 1758–1775 (1999).
16. Stradi, D. *et al.* Role of dispersion forces in the structure of monolayer graphene on Ru surfaces. *Phys. Rev. Lett.* **106,** 186102 (2010).
17. Stradi, D. *et al.* Electron localization in epitaxial graphene on Ru(0001) determined by moiré corrugation. *Phys. Rev. B* **85,** 121404R (2012).
18. Tang, W., Sanville, E. & Henkelman, G. A grid-based Bader analysis algorithm without lattice bias. *J. Phys. Condens. Matter* **21,** 084204 (2009).
19. Repp, J. *et al.* Imaging Bond formation between a gold atom and pentacene on an insulating surface. *Science* **312,** 1196–1199 (2006).
20. Kondo, J. Effect of ordinary scattering on exchange scattering from magnetic impurity in metals. *Phys. Rev.* **169,** 437–440 (1968).
21. Li, J. *et al.* Kondo scattering observed at a single magnetic impurity. *Phys. Rev. Lett.* **80,** 2893–2896 (1998).
22. Madhavan, V. *et al.* Tunneling into a single magnetic atom: Spectroscopic evidence of the Kondo resonance. *Science* **280,** 567–569 (1998).
23. Nagaoka, K. *et al.* Temperature dependence of a single Kondo impurity. *Phys. Rev. Lett.* **88,** 077205 (2002).
24. Ternes, M., Heinrich, A. J. & Schneider, W-D. Spectroscopic manifestations of the Kondo effect on single adatoms. *J. Phys. Condens. Matter* **21,** 053001 (2009).
25. Iancu, V., Deshpande, A. & Hla, S-W. Manipulation of the Kondo effect via two-dimensional molecular assembly. *Phys. Rev. Lett.* **97,** 266603 (2008).
26. Fernández Torrente, I. *et al.* Vibrational Kondo effect in pure organic charge transfer assemblies. *Phys. Rev. Lett.* **101,** 217203 (2008).
27. Temirov, R., Lassise, A., Anders, F. B. & Tautz, F. S. Kondo effect by controlled cleavage of a single-molecule contact. *Nanotechnology* **19,** 065401 (2008).
28. Choi, T. *et al.* A single molecule Kondo switch: Multistability of tetracyanoethylene on Cu(111). *Nano Lett.* **10,** 4175–4180 (2010).
29. Komeda, T. *et al.* Observation and electric current control of a local spin in a single-molecule magnet. *Nature Commun.* **2,** 217 (2011).
30. Tasaki, H. Ferromagnetism in the Hubbard models with degenerate single electron ground states. *Phys. Rev. Lett.* **69,** 1608–1611 (1992).
31. Mielke, A. Ferromagnetism in single band Hubbard models with a partially flat band. *Phys. Rev. Lett.* **82,** 4312–4315 (1999).
32. Nagaoka, Y. Ferromagnetism in a narrow, half-filled band. *Phys. Rev.* **147,** 392–405 (1966).
33. Arita, R. *et al.* Gate induced band ferromagnetism in an organic polymer. *Phys. Rev. Lett.* **88,** 127202 (2002).
34. Wiesendanger, R. Spin mapping at the nanoscale and atomic scale. *Rev. Mod. Phys.* **81,** 1495–1550 (2009).

Acknowledgements

Financial support by the Ministerio de Educación y Ciencia through projects CONSOLIDER-INGENIO 2010 on Molecular Nanoscience, FIS2010-18847, FIS2010-15127 and CTQ2010-17006 and Comunidad de Madrid through the programme NANOBIOMAGNET S2009/MAT1726 is gratefully acknowledged. S.B. would like to acknowledge the FPU Grant AP-2007-001157. D.S. and M.G. would like to acknowledge the FPI-UAM programme.

Author contributions

The experiments were carried out primarily by M.G. and S.B., with important contributions by F.C. The calculations were performed mainly by D.S. with contributions by C.D. and M.A., and F.M. leading the theoretical approach. N.M. selected the specific chemical system. The data analysis was carried out by A.L.V.d.P., who also contributed to the writing of the manuscript. R.M. developed the physical idea and wrote the paper.

Additional information

Supplementary information is available in the online version of the paper. Reprints and permissions information is available online at www.nature.com/reprints. Correspondence and requests for materials should be addressed to A.L.V.d.P.

Competing financial interests

The authors declare no competing financial interests.